

# Harmonic Balance Solutions of Realistic Rotor Configurations

M.A.Woodgate and G.N.Barakos

CFD Laboratory, School of Engineering  
University of Liverpool, L69 3GH, U.K.

<http://www.liv.ac.uk/engdept>

Email: [G.Barakos@liverpool.ac.uk](mailto:G.Barakos@liverpool.ac.uk)

## Abstract

Computational fluid dynamics (CFD) based on the Navier-Stokes equations is nowadays used by the rotorcraft industry for the analysis and design of helicopter rotors. Computations for rotor axial flight benefit from the use of a rotating frame of reference that leads to steady-flow equations and avoids expensive time-marching CFD analyses. For rotors in forward flight, efficient computations could be made by solving the governing equations in the frequency domain assuming that the flow is periodic. This type of analysis is more efficient in terms of CPU time but requires more memory for the computations. In this paper, a frequency-domain CFD method developed by the authors is demonstrated for demanding rotor cases and is compared against time-marching analysis at the same conditions.

## 1 INTRODUCTION

Within the rotorcraft CFD domain, several works are currently available in the open literature with good demonstrations of the accuracy of Navier-Stokes-based methods for rotors in forward flight [18]. In addition, CFD works considering rotor-fuselage and complete helicopter configurations also begin to appear [17]. The main drawback of these methods is most of the times associated with the excessive CPU cost needed to resolve the rotor flow and provide data for several azimuth angles. This cost is associated with time-marching solutions that need small steps in azimuth and several rotor revolutions to reach a converged state. An alternative would be to solve for the rotor flow using frequency domain or time-linearised methods that are popular within the domain of turbo-machinery research [12]. This challenging task to compute rotors with non time-marching methods has so far been addressed by few authors [4, 6, 7, 10, 11].

The work of Butsumtorn and Jameson [4] for example, relies on the solution of the Navier-Stokes equations on the frequency domain and requires Fourier Transformations within the iterative numerical process. The work of Ekici et al. [10] is an extension of the well-known method of harmonic balance, that is popular within the aero-elasticity domain. The time spectral approach of Gopinath and Jameson [11], has been applied to rotors by Butsumtorn and Jameson [4], and Choi has also used the time spectral method to predict rotor loads [6] [7]. Most of these works, however, originate from explicit time-marching schemes and remain explicit in their nature when transformed to the frequency domain. Dufour *et al.* [9] compared the performance and accuracy of both Linearised and Harmonic balance methods within the CFD code elsA [5] to predict the unsteady aerodynamic loads for an airfoil with a flap at subsonic and transonic flows. It was reported, for the subsonic cases, that the linearised method performed well. However, in the transonic regime the accuracy deteriorated and the single mode harmonic balance method always produced a more accurate answer at the expense of more computational cost.

In the present work, a method is proposed that enables the

use of non-time-marching methods within the framework of implicit flow solvers. The scheme maintains good compatibility with existing time-marching implicit flow solvers and is relatively easy to implement. To demonstrate this approach, the Helicopter Multi-block Solver (HMB) of Liverpool [3, 17] is used. After implementation, the method is demonstrated for a range of test cases including oscillating aerofoils, aerofoils in pitch-translation oscillation as well as non-lifting and lifting rotors in forward flight. The cases are selected to increase in complexity to demonstrate the limitations and costs of the harmonic balance method. Where appropriate, the results are compared with time-marching solutions obtained with the same CFD code.

## 2 NUMERICAL METHODS

### 2.1 Helicopter Multi-Block solver

The Helicopter Multi-Block(HMB) code, developed at Liverpool can solve the Navier-Stokes equations in integral form using the arbitrary Lagrangian Eulerian (ALE) formulation for time-dependent domains with moving boundaries:

$$\frac{d}{dt} \int_{V(t)} \vec{w} dV + \int_{\partial V(t)} \left( \vec{F}_i(\vec{w}) - \vec{F}_v(\vec{w}) \right) \vec{n} dS = \vec{S} \quad (1)$$

where  $V(t)$  is the time dependent control volume,  $\partial V(t)$  its boundary,  $\vec{w}$  is the vector of conserved variables  $[\rho, \rho u, \rho v, \rho w, \rho E]^T$ .  $\vec{F}_i$  and  $\vec{F}_v$  are the inviscid and viscous fluxes, including the effects of the time dependent domain. For hovering rotor simulations, the grid is fixed and a source term  $\vec{S} = [0, -\rho \vec{\omega} \times \vec{u}_h, 0]^T$  is added to compensate for the inertial effects of the rotation.  $\vec{u}_h$  is the local velocity field in the rotor-fixed frame of reference.

The Navier-Stokes equation are discretised using a cell-centred finite volume approach on a multi-block grid, leading to the following equations:

$$\frac{\partial}{\partial t} (\mathbf{w}_{i,j,k} V_{i,j,k}) = -\mathbf{R}_{i,j,k}(\mathbf{w}_{i,j,k}) \quad (2)$$

where  $\mathbf{w}$  represents the cell variables and  $\mathbf{R}$  the residuals.  $i, j$  and  $k$  are the cell indices and  $V_{i,j,k}$  is the cell volume. Osher's [14] upwind scheme is used to discretise the convective terms and MUSCL variable interpolation is used to provide third order accuracy. Van Albada limiter is used to reduce the oscillations near steep gradients.

Temporal integration is performed using an implicit dual-time step method. The linearised system is solved using the generalised conjugate gradient method with a block incomplete lower-upper (BILU) pre-conditioner [1].

Multi-block structured meshes are used for HMB. These meshes are generated using ICEM-Hexa<sup>TM</sup> of Ansys. The multi-block topology allows for an easy sharing of the calculation load for parallel computing. Adding sliding meshes [17], as well as allowing for mesh overlap makes the HMB a very flexible solver for dealing with complex geometries. Given the existing data structure of the solver, the modifications required for the mesh overlap were restricted to a small part of the code. Within HMB, halo cells are employed by each block, and are populated from boundary conditions, bloc-to-block data exchanges, data from sliding surfaces or data from overlapping meshes. For as long as a block has correct information on the halo cells, its solution can be updated and then shared with other neighbouring blocks. In the strongly implicit HMB method, only the preconditioner employed for the solution of the linear system of equations is decoupled between blocks. For overlap regions though and to minimise the exchange of data, the Jacobian matrix is also de-coupled for overlapping mesh regions. Another necessary modification for the solution on overlapping grids is related to the treatment of cells marked as holes. These are identified and kept in the original system of equations even if their solution is not to be updated. This allows for the structure of the solver to remain the same and has minimal overhead in the computation.

## 2.2 Harmonic Balance

An alternative to time marching, is the Harmonic Balance method that allows for a direct calculation of the periodic state. Starting from the semi-discrete form as a system of ordinary differential equations:

$$I(t) = V \frac{dW(t)}{dt} + R(t) = 0, \quad (3)$$

and considering the solution  $W$  and the residual  $R$  to be periodic in time and functions of the frequency  $\omega_i$ ,

$$W(t) = \sum_{k=-\infty}^{\infty} \hat{W}_k e^{ik\omega t}, \quad (4)$$

$$R(t) = \sum_{k=-\infty}^{\infty} \hat{R}_k e^{ik\omega t} \quad (5)$$

we can truncate the series to a specified number of harmonics  $N_H$ :

$$W(t) = \sum_{k=-N_H}^{N_H} \hat{W}_k e^{ik\omega t}, \quad (6)$$

$$R(t) = \sum_{k=-N_H}^{N_H} \hat{R}_k e^{ik\omega t}. \quad (7)$$

Then equation (3) can also be truncated using a Fourier series expansion,

$$I(t) = \sum_{k=-N_H}^{N_H} \hat{I}_k e^{ik\omega t}. \quad (8)$$

The discrete Fourier transforms can be substituted into the semi-discrete form equation (3) with the time derivative of the state variables pushed inside the series summation. Using the orthogonality of the Fourier terms results in an equation for each wave number  $k$

$$i\omega k V \hat{W}_k + \hat{R}_k = 0. \quad (9)$$

It should be noted that since  $R(W(t))$  is a non linear function of  $W(t)$  then each coefficient  $\hat{R}_k$  depends on all the coefficient  $\hat{W}_k$ . Hence equation 9 represents a non-linear system of equations which must be solved iteratively so

$$\hat{I}_k = i\omega k V \hat{W}_k + \hat{R}_k = 0. \quad (10)$$

The system is  $N_T = 2N_H + 1$  equations in  $N_H$  unknown harmonics and can be expressed as

$$\omega A \hat{W} + \hat{R} = 0 \quad (11)$$

where  $A$  is a  $N_T \times N_T$  matrix. There are several approaches to calculating the residual in the frequency domain. The first approach is to attempt to form an analytical expression between  $\hat{R}_k$  and  $\hat{W}_k$ . This approach requires a complex series of convolution sums to calculate  $\hat{R}_k$  directly from  $\hat{W}_k$ . Hall [12] rightly discards this approach due to its massive complexity and the fact that the cost scales quadratically with the number of modes. The alternative approach by Hall was to use the pseudo-spectral approach in the time domain while McMullen *et. al.* [13] employs a similar approach in the frequency domain.

### 2.2.1 Pseudo Spectral Approach in the Time Domain

In the approach of Hall instead of solving (9) directly in the frequency domain, the equation is transformed back into the time domain. The solution is split into  $N_T$  discrete equally spaced sub intervals over the period  $T = 2\pi/\omega$

$$W_{hb} = \begin{pmatrix} W(t_0 + \Delta t) \\ W(t_0 + 2\Delta t) \\ \vdots \\ W(t_0 + T) \end{pmatrix} \quad R_{hb} = \begin{pmatrix} R(t_0 + \Delta t) \\ R(t_0 + 2\Delta t) \\ \vdots \\ R(t_0 + T) \end{pmatrix} \quad (12)$$

where  $\Delta t = 2\pi/(N_T\omega)$ . Then, there exists a transformation matrix [20]  $E$  such that

$$\hat{W} = EW_{hb} \quad \text{and} \quad \hat{R} = ER_{hb}$$

and equation (11) becomes

$$\omega AEW_{hb} + ER_{hb} = 0 = \omega E^{-1}AEW_{hb} + E^{-1}ER_{hb} = \omega DW_{hb} + R_{hb} \quad (13)$$

with  $D = E^{-1}AE$  and the components of  $D$  are defined by

$$D_{i,j} = \frac{2}{N_T} \sum_{k=1}^{N_H} k \sin(2\pi k(j-i)/N_T).$$

Note that the diagonal  $D_{i,i}$  is zero. We can then apply pseudo time marching to the harmonic balance equation

$$\frac{dW_{hb}}{dt} + \omega DW_{hb} + R_{hb} = 0 \quad (14)$$

This equation is solved using an implicit method, a step of which is written as

$$\frac{W_{hb}^{n+1} - W_{hb}^n}{\Delta t^*} = - [\omega DW_{hb}^n + R_{hb}(W_{hb}^{n+1})] \quad (15)$$

### 2.2.2 Explicit Source Term

Returning to the system of equations (15)

$$\frac{dW_{hb}}{dt} + \omega DW_{hb} + R_{hb} = 0. \quad (16)$$

The first method is to only treat implicitly the residual  $R_{hb}$  but not the source term  $\omega DW_{hb}$

$$\frac{W_{hb}^{n+1} - W_{hb}^n}{\Delta t^*} = - [\omega DW_{hb}^n + R_{hb}(W_{hb}^{n+1})] = \frac{\Delta W_{hb}}{\Delta t^*}. \quad (17)$$

This leads to the linear system

$$\begin{bmatrix} \frac{R}{W} \Big|_{t_0+\Delta t} & 0 & \dots & 0 \\ 0 & \frac{R}{W} \Big|_{t_0+2\Delta t} & & \\ \vdots & & \ddots & \\ 0 & 0 & & \frac{R}{W} \Big|_{t_0+T} \end{bmatrix} \cdot \quad (18)$$

$$= \begin{bmatrix} \Delta W(t_0 + \Delta t) \\ \Delta W(t_0 + 2\Delta t) \\ \vdots \\ \Delta W(t_0 + T) \end{bmatrix} - \begin{bmatrix} R(t_0 + \Delta t) \\ R(t_0 + 2\Delta t) \\ \vdots \\ R(t_0 + T) \end{bmatrix} - \omega \begin{bmatrix} D_{1,j} W_{hb} \\ D_{2,j} W_{hb} \\ \vdots \\ D_{N_T,j} W_{hb} \end{bmatrix}.$$

The right hand side is just the standard residual operator calculated at the  $i$ th snapshot plus the approximation of the source term. The left hand side is just the standard Jacobian operator calculated at the  $i$ th snapshot. The matrix is block diagonal and can be solved independently of each of the  $N_T$  instances. Hence  $N_T$  steady flows are computed and they are only coupled through the Fourier approximation of the unsteady residual of the discretised system. This method has one very clear advantage in that only the  $i$ th snapshot of the Jacobian has to be stored at once so not extra memory is required for the linear solver over the standard method. However, the explicit treatment of the source term is likely to restrict the size of the CFL number and this problem intensifies with the number of modes used.

### 2.2.3 Implicit Source Term

There are a number of ways to treat the source term within the Harmonic balance framework. Sicot *et al.* [16] apply an

iterative block-Jacobi method to move the implicit coupling from the Jacobian matrix to the right hand side to maintain the  $2N_H + 1$  independent linear systems of the explicit at the cost of having to do several sweeps to ensure the implicit coupling effect is introduced. In this work, and in order to increase the size of the usable CFL number and allow for more modes an implicit treatment of the source term was used.

$$\omega DW_{hb}^{n+1} = \omega DW_{hb}^n + \omega D(\Delta W_{hb}). \quad (19)$$

The unsteady term couples together the variables at all  $N_T$  snapshots which leads to a coupling of the increments also Equation (14) then becomes:

$$\frac{W_{hb}^{n+1} - W_{hb}^n}{\Delta t^*} = - [\omega DW_{hb}^{n+1} + R_{hb}(W_{hb}^{n+1})] \quad (20)$$

The Jacobian matrix  $J$  is

$$J = \begin{bmatrix} \frac{R}{W} \Big|_{t_0+\Delta t} & \omega D_{1,2} & \dots & \omega D_{1,N_T} \\ \omega D_{2,1} & \frac{R}{W} \Big|_{t_0+2\Delta t} & & \\ \vdots & & \ddots & \\ \omega D_{N_T,1} & \omega D_{N_T,2} & & \frac{R}{W} \Big|_{t_0+T} \end{bmatrix} \quad (21)$$

where  $\partial R/\partial W$  is the Jacobian matrix of the CFD residual and the linear system that needs to be solved is

$$\left[ \frac{V}{\Delta t^*} + J \right] \Delta W_{hb} = -R_{hb}^n - \omega DW_{hb}^n \quad (22)$$

where  $V$  is the cell volume.

There are two considerations when solving equation (22). Firstly, for solving the CFD system it is normally more efficient, CPU time wise, to use an approximate Jacobian matrix based on a lower-order spatial discretisation of the residual function. This results in a linear system that has less terms in the coefficient matrix and is better conditioned due to be more diagonally dominant. Then, a sparse matrix solver is used to calculate the updates from the solution of the linear system. For solving the harmonic balance system several experiments were made based on experience with solving for a CFD steady state. First, for the terms on the diagonal of  $J$ , arising from the CFD residual, an approximate Jacobian matrix arising from the first-order discretisation of  $R$  is used. The linear system is solved using a Krylov subspace method with BILU factorisation with no fill-in. This is effective for systems arising from CFD [2].

The drawback of the fully implicit method is its memory footprint that increases faster than  $2N_H + 1$  times the steady state solver requirements. This is due to the extra memory needed to store the off-diagonal blocks of the preconditioner. There are several possible methods for calculating the initial estimates of these  $2N_H + 1$  snapshots. These range from using initial freestream values to calculating  $2N_H + 1$  steady state solves with the mesh in the correctly deformed position with the correct grid velocities, i.e. setting the unsteady source term of equation (20) to zero. For the harmonic balance results shown below we have used the later which it provides a better initial guess and enhances the robustness of the implicit solve during the initial iterations.

### 3 RESULTS AND DISCUSSION

The first test for the harmonic balance, was the well-known AGARD CT1 oscillating aerofoil case (freestream Mach number of 0.6, mean incidence  $\alpha_m = 2.89$ , reduced frequency of  $k = 0.0808$ , and amplitude of oscillation of  $\alpha_0 = 2.41$  degrees, pitching about the quarter chord) and proved to be well-resolved by the harmonic balance method. Figure 1 shows the comparison between the time marching and the harmonic balance results. There is only a tiny difference between the pressure field of the non linear time marching method and the single-mode harmonic balance solution, and the lift and the drag are well predicted even with a very small number of modes. The AGARD CT5 case, proved much more challenging since a larger hysteresis is expected for the integrated loads. As can be seen in Figure 2, the solution with one mode correctly predicts the single shock on the lower side but the shock is too far forward. Adding a second mode greatly improves the behaviour but the shock is still not correctly captured. This does not improve much with the addition of the 3rd and 4th modes. However, by the time the 5th mode is added the two solutions only have minor differences. Figure 3 shows the lift which is well predicted even with a small number of modes and the moment, which is much more sensitive to shock location and strength. There is a much wider scatter around the non-linear time-marching result. The convergence history of the harmonic balance method for the CT5 case is shown in Figure 3(c).

The addition of a translational motion to the aerofoil, which induces an effective change in Mach number, makes capturing the flow features difficult. The inviscid and turbulent cases computed here, both use the same pitch schedule shown in Figure 4. Though this schedule is dominated by a once per cycle sine component it also has a number of higher frequencies as one would expect for a rotor section in forward flight. This implies that the pitch schedule itself will in effect only be approximate for a low number of modes. The use of a two equation turbulence model also presented challenges since with the  $k - \omega$  model, positivity of  $k$  and  $\omega$  was maintained at each iteration by resetting the values of  $k$  and  $\omega$  to the initial free-stream values if they went negative. Figure 5 shows the comparison between the lift and drag of the time marching and the 7-mode harmonic balance solutions. The results suggest excellent agreement between the methods for the lift and drag throughout the cycle. Figure 6 shows the convergence of drag for the 7-mode case against iteration number. Since there are 7 modes there are 15 snapshots and hence 15 drag predictions during the oscillation. Within 1,000 iterations the drag of all the snapshots has settled down. The convergence histories of the flow residuals can also be seen in Figure 7. Finally, a comparison of the Mach number fields of the non linear time marching and 7-mode harmonic balance solutions is shown in Figure 8. The shock strength is slight over-predicted and is too far forward compared to the time marching on the advancing side however the agreement on the retreating side is excellent.

The rotor cases for the Harmonic balance method include the ONERA non-lifting rotor of [19], the fully articulated case reported in [15], and the UH60-A [8] rotor in fast forward flight. The ONERA non-lifting rotor was run inviscid with 7 modes. A comparison between the surface pressure on the

blades can be seen in Figure 9. The differences between the two solutions are more closely examined in Figure 10 at four different azimuth angles. On the advancing side, the surface pressure near the blade root is well captured. Near the tip, however, the shock is very slightly aft of the non-linear time marching solution and has its strength mildly over-predicted. On the retreating side, the blade tip is better resolved with the blade root showing the largest differences between the time marching results and the 7-mode harmonic balance solutions. Figure 11 shows sectional plots at 76% of the blade radius for the surface pressure coefficient at three azimuth angles. The time-marching and the harmonic balance results agree quite well with minor differences observed near the strong shock on this blade. A Mesh of 2.15 million cells and 236 blocks was used and the calculation was run in parallel on 80 processors.

The second rotor case concerns a fully articulated rotor. The inviscid mesh for this case contained 1.05 million cells, 236 blocks and was computed on 100 processors. A viscous mesh for the same test case contained 6.08 million cells, 272 blocks and was run on 80 processors. For this case, the mesh had to be deformed to account for the blade pitching and flapping and so the volume changes between the cells at different time snapshots have to be taken into account. Figure 12 compares the surface pressure on the blades between the inviscid, non-linear time-marching solution, a 7-mode inviscid harmonic balance solution and a 2-mode viscous harmonic balance solution. The viscous effects are small in this case and hence all three solutions are in close agreement. The rotor was run at a tip Mach number of 0.6, a Reynolds number of half a million, advance ratio  $\mu = 0.25$  and shaft angle of  $-3.0$  degrees. The trim condition set the collective to 4.0 degrees, a coning angle of 1.5 degrees, a single flap harmonic with 2.0 degrees for the *cos* term and 2.0 degrees for the *sin* term, a single pitch harmonic of 2.0 degrees for the *sin* term and a single lag harmonic of  $-2.0$  for the *sin* term.

The more challenging case computed with the harmonic balance method is the forward flying UH60A rotor. The blade was articulated and a blade deformation was also imposed on the mesh according to the results reported by Datta and Chopra [8] and previous computations with HMB for this case [18]. The rotor was run at a tip Mach number of 0.642, a Reynolds number of half a million, advance ratio  $\mu = 0.368$  and shaft angle of  $-7.31$  degrees. The trim condition set the collective to 11.6 degrees, the coning angle to 3.43 degrees, a single flap harmonic with  $-0.7$  degrees for the *cos* term and  $-1.0$  for the *sin* term, a single pitch harmonic of  $-2.39$  degrees for the *cos* term and 8.63 degrees for the *sin* term and no lag harmonics.

Figure 13 compares the surface pressure on the blades between the 2- and 4-mode harmonic balance solutions and the non-linear time-marching results. The 2-mode solution of a 4-bladed rotor has a representation of a blade every 18 degrees of azimuth while the 4-mode solution resolution is nearly double that at 10 degrees. Overall, the solutions show good qualitative agreement. Figure 14 shows a quantitative comparison of the pressure at 3 different azimuths. Figure 15 shows the comparison of the surface  $C_p$  at the 67.5%*R* station, and at every 90 degrees of azimuth. Figure 16 shows the comparison of Mach squared scaled loads between the exper-



imental data, non-linear time-marching and the 4-mode harmonic balance methods. This is a very demanding test case, and the results show good agreement between the CFD and the experiments as well as a fair agreement between the time-marching and harmonic balance solutions. For this case, the memory requirement for the HB method was 95 GBytes for the 2-mode case and 219 GBytes for the 4-mode case. The time marching solution required 3 rotor revolutions of 1440 time steps, and a total CPU time of 9.8 days on 128 Pentium nodes. The 2-mode harmonic balance required a total time of just one day while the 4-mode harmonic balance required 2.6 days on the same system and grid as the time-marching.

The main drawback of the fully implicit harmonic balance method is the memory footprint. The ideal scaling would be  $2N_H + 1$  however, the employed Jacobian and preconditioner matrices grow at a faster rate. The growth, is due to the off diagonal terms added in from the implicit source term which cause the increased scaling. For  $N_H$  modes there are  $2N_H(2N_H + 1)$  of them but since there are 7 blocks in the approximate Jacobian the real scaling over the steady state method is  $2N_H + 1 + 2N_H(2N_H + 1)/7$ . Table 1 shows the scaling for the first 7 modes. For up to about 4 or 5 modes the performance is not too bad. However for 7 modes, the memory is already at 3 times the ideal scaling and gets worst progressively.

#### 4 CONCLUSIONS AND FUTURE WORK

A method suitable for fast analysis of rotor flows was presented and assessed in this paper. Across the board of the AGARD CT cases, the method produced results in excellent agreement with time-marching computations. The in-plane translation was also well-resolved and a modest number of flow modes was adequate for predictions of good engineering accuracy. The method is more expensive in terms of computer memory than time-marching CFD algorithms, and requires careful implementation for efficient computations. The results, however, are more than satisfactory. As part of this work, inviscid and viscous test cases were assessed and the harmonic balance method produced excellent results for the non-lifting ONERA rotor at high blade advance ratio. The same was true for a lifting rotor with articulation that was assessed in forward flight as well as the UH60A rotor in high speed. It is evident from the current work that the harmonic balance method is adequate for many engineering computations and with a reduction in the required computer memory this technique has the potential to change the way time-marching is used in CFD for engineering analysis of rotors. Following this work, further efforts are directed towards expanding the method, reducing its memory footprint and demonstrating more complex flow cases.

#### Acknowledgements

The financial support via the REACT project of AgustaWestland and the Business Innovation and Skills Department of UK is gratefully acknowledged.

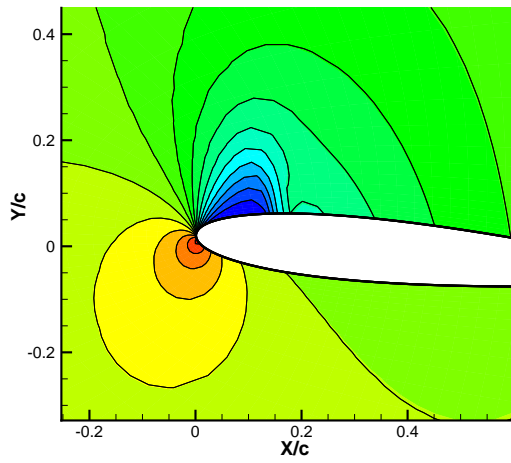
#### REFERENCES

- [1] O. Axelsson. *Iterative Solution Methods*. Cambridge University Press: Cambridge, MA, 1994.
- [2] K.J. Badcock, B.E. Richards, and M.A. Woodgate. Elements of computational fluid dynamics on block structured grids using implicit solvers. *Progress in Aerospace Sciences*, 36:351–392, 2000.
- [3] G. Barakos, R. Steijl, K. Badcock, and A. Brocklehurst. Development of CFD Capability for Full Helicopter Engineering Analysis. 31st European Rotorcraft Forum, 13-15 September 2005, Florence, Italy, 2005.
- [4] N. Butsumtorn and A. Jameson. Time spectral method for rotorcraft flow. In *AIAA Paper 2008-0403*, Reno, Nevada, 7-10 January 2008. 46th AIAA Aerospace Sciences Meeting and Exhibit.
- [5] L. Cambier and J.-P. Veuillot. Status of the elsA CFD software for flow simulation and multidisciplinary applications. *AIAA Paper 2008-664*, 46th Aerospace Sciences Meeting and Exhibit, Reno, Nevada, January 7-10, 2008.
- [6] S. Choi and A. Datta. Cfd prediction of rotor loads using time-spectral method and exact fluid-structure interface. In *AIAA Paper 2008-7325*, Honolulu, Hawaii, 18-21 August 2008. 26th AIAA Applied Aerodynamics Conference.
- [7] S. Choi, M. Postdam, K. Lee, G. Iaccarino, and J. Alonso. Helicopter rotor design using a time-spectral and adjoint-based method. In *AIAA Paper 2008-5810*, British Columbia, Canada, 10-12 September 2008. 12th AIAA/ISSMO Multidisciplinary Analysis and Optimization Conference.
- [8] A. Datta and I. Chopra. Validation of structural and aerodynamic modeling using uh-60a flight test data. American Helicopter Society 59th Annual Forum, Phoenix, May 6-8, 2003.
- [9] G. Dufour, F. Sicot, G. Puigt, C. Liauzun, and A. Dugeai. Contrasting the harmonic balance and linearized methods for oscillating-flap simulations. *AIAA Journal*, 48(9):788–797, 2010.
- [10] K. Ekici, K.C. Hall, and E.H. Dowell. Computationally Fast Harmonic Balance Methods for Unsteady Aerodynamic Predictions of Helicopter Rotors. *Journal of Computational Physics*, 227:6206–6225, 2008.
- [11] A. K. Gopinath and A. Jameson. Time spectral method for periodic unsteady computations over two- and three-dimensional bodies. In *AIAA Paper 2005-1220*, Reno, Nevada, 10-13 January 2005. 43th AIAA Aerospace Sciences Meeting and Exhibit.
- [12] K.C. Hall, W.S. Clark, and C.B. Lorence. A linearized Euler analysis of unsteady transonic flows in turbomachinery. *Journal of Turbomachinery*, 116(3):477–488, 1994.

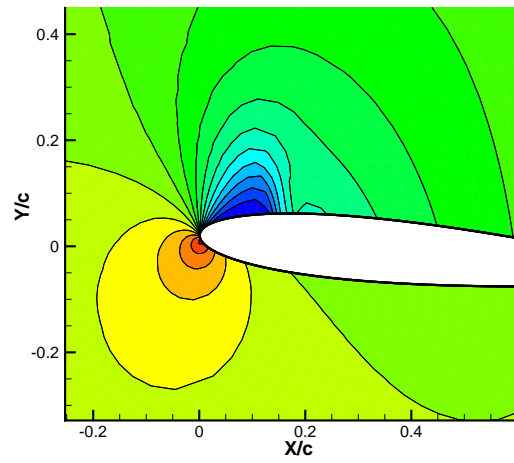
$N_H$	1	2	3	4	5	6	7
$2N_H + 1$	3	5	7	9	11	13	15
$2N_H + 1 + 2N_H(2N_H + 1)/7$	3.86	7.86	13.0	19.2	26.7	35.3	45.0

Table 1: The scaling for the memory for the Harmonic Balance case with  $N_H$  Modes

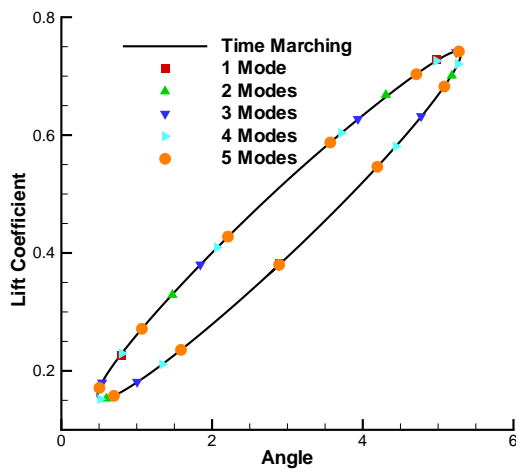
- [13] M. MacMullen. The application of non-linear frequency domain methods to the euler and navier-stokes equations. PhD dissertation, Stanford University, CA, USA, 2003.
- [14] S. Osher and S. Chakravarthy. Upwind Schemes and Boundary Conditions with Applications to Euler Equations in General Geometries. *Journal of Computational Physics*, 50(3):447–481, June 1983.
- [15] R. Steijl, G. Barakos and K. Badcock. A framework for CFD analysis of helicopter rotors in hover and forward flight. *International Journal for Numerical Methods in Fluids*, 51(8):819–847, 2006.
- [16] F. Sicot, G. Puigt, and M. Montagnac. Block-jacobi implicit algorithms for the time spectral method. *AIAA Journal*, 46(12):3080–3089, 2009.
- [17] R. Steijl and G. Barakos. Sliding Mesh Algorithm for CFD Analysis of Helicopter Rotor-Fuselage Aerodynamics. *Int. J. Numer. Meth. Fluids*, 58:527–549, 2008.
- [18] R. Steijl and G.N. Barakos. A Computational Study of the Advancing Side Lift Phase Problem. *Journal of Aircraft*, 45(1):246–257, 2008.
- [19] M.E. Tauber, I-Chung Chang, D.A. Caughey, and J-J Philippe. Comparison of calculated and measured pressures on straight- and swept-tip model rotor blades. Technical Report TM-85872, NASA, 1983.
- [20] J. P. Thomas, E. H. Dowell, K. C. Hall, and C. M. Dene-gri. Further investigation of modeling limit cycle oscillation behaviour of the F-16 fighter using a harmonic balance approach. In *AIAA Paper 2005-1917*, Austin, TX, April 2005. 46th AIAA/ASME/ASCE/AHS/ASC Structures, Structural Dynamics and Materials (SDM) conference.



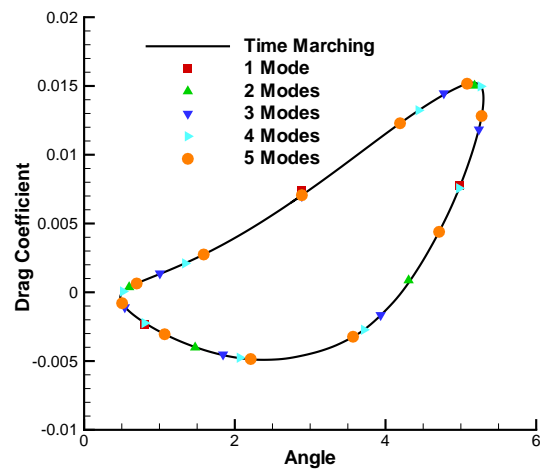
1-Mode



4-Modes



Lift coefficient



Drag coefficient

Figure 1: Comparison of the time marching results (shaded contours) and the harmonic balance pressure (black solid lines) for the flow field of the CT1 test case, at 4.98 degrees down. The lift and drag hysteresis are also shown for up to 5 modes.

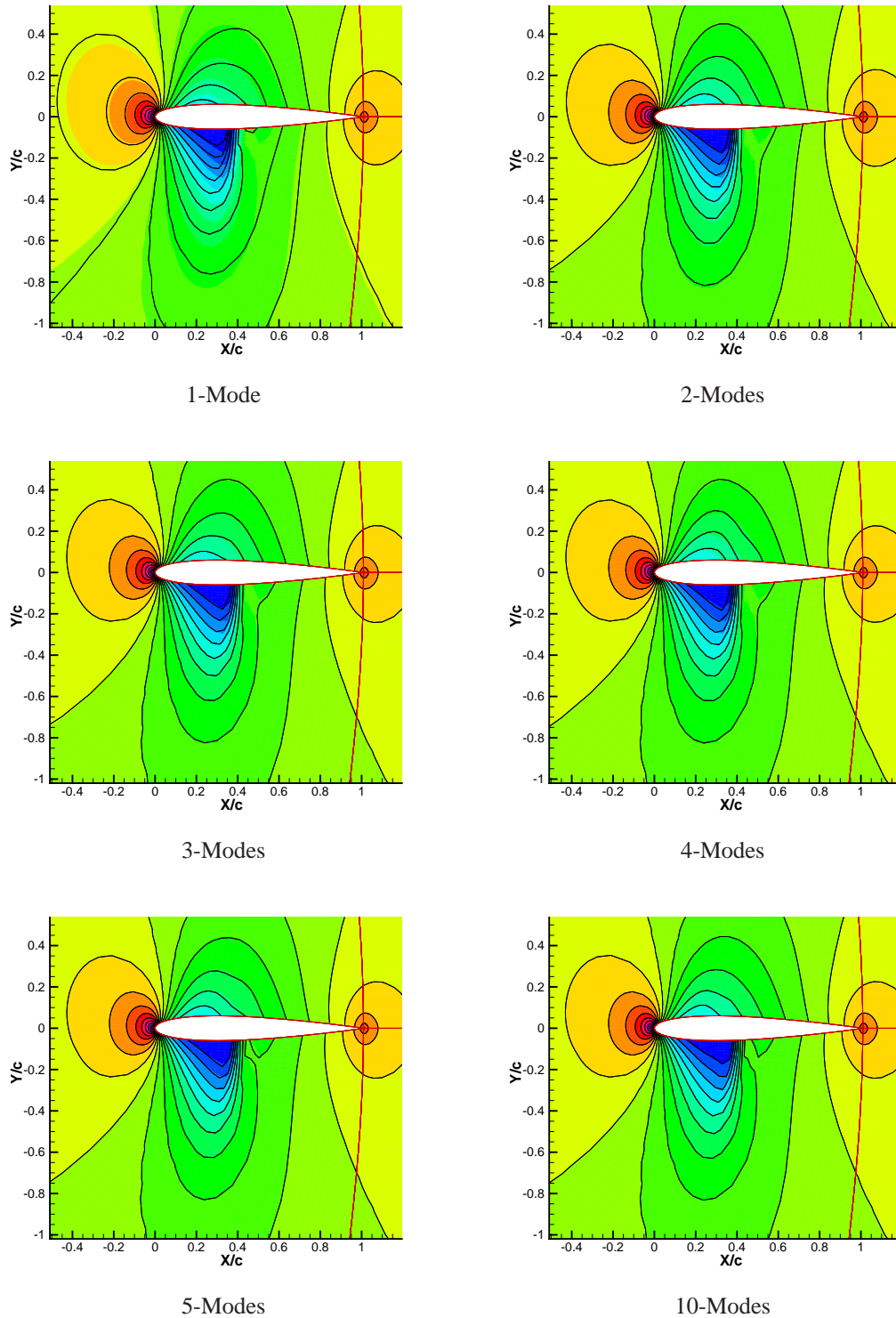
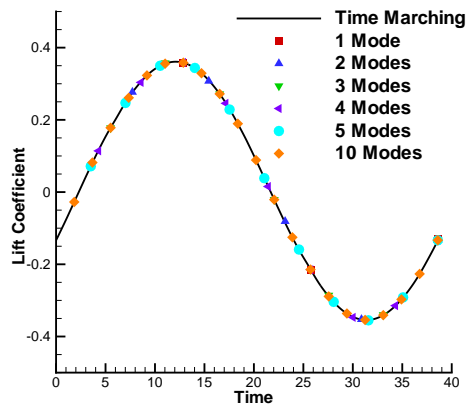
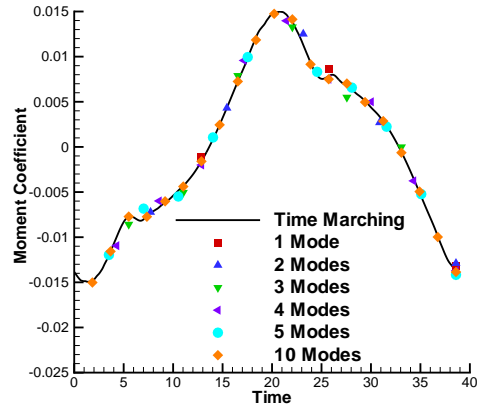


Figure 2: Comparison of the time marching results (shaded contours) and the harmonic balance pressure ( black solid lines) for the flow field of the CT5 test case.

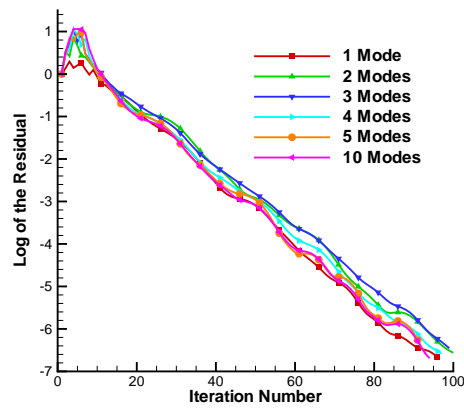




(a) Lift coefficient



(b) Moment coefficient



(c) Convergence history

Figure 3: (a,b) Evolution of loads of the time marching (solid line) and the harmonic balance solutions for the CT5 test case. (c) Convergence history for the harmonic balance method.

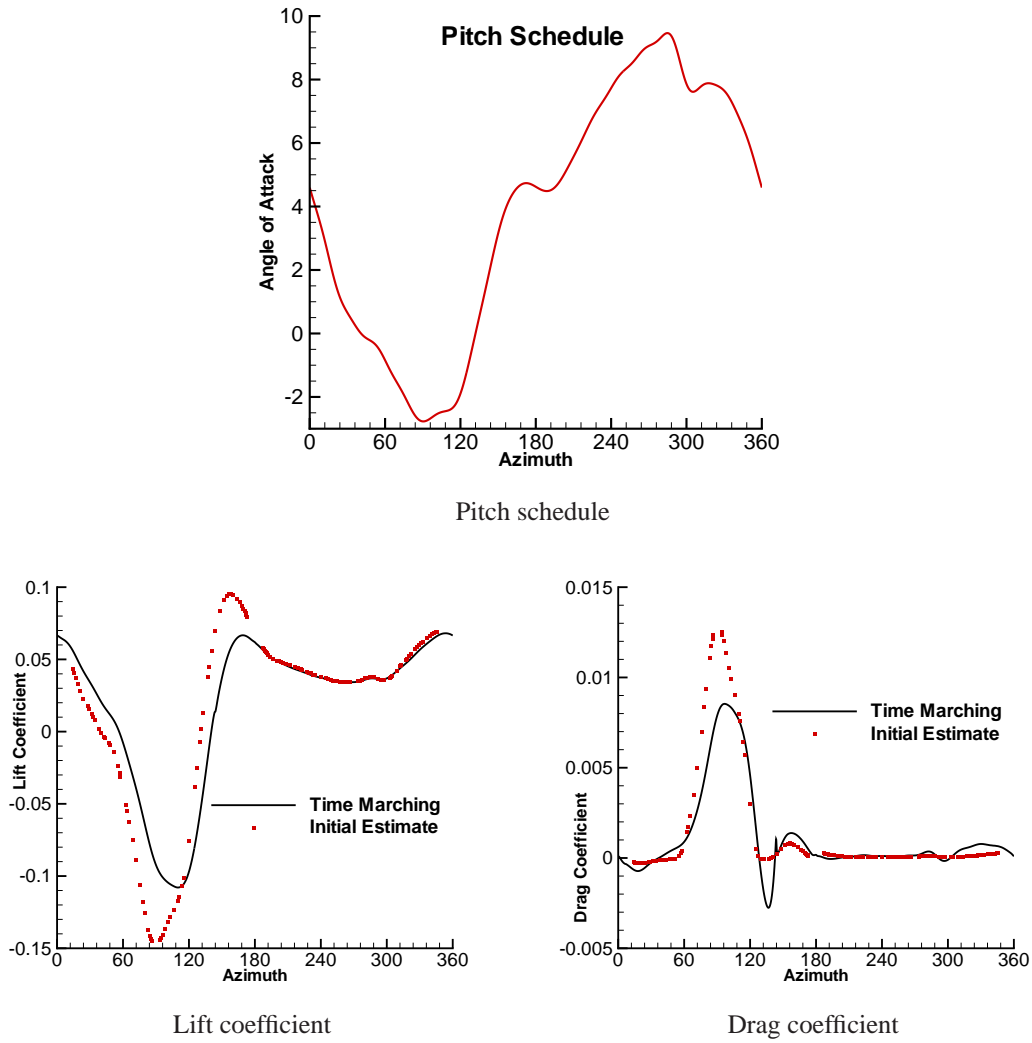


Figure 4: Pitch schedule and comparison of the non linear time marching (solid line) and the initial loads estimates for the harmonic balance of the inviscid dMdt test case ( $M_\infty = 0.55$ ,  $\mu = 0.45$  and  $k = 0.3668$ ).

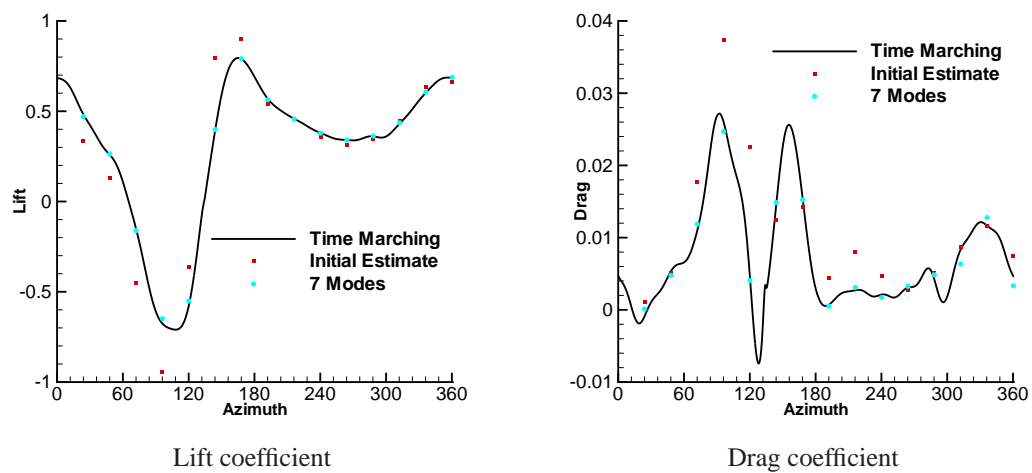


Figure 5: Comparison of the time marching (solid line) and the 7-mode harmonic balance solutions for the loads for the viscous dMdt case ( $M_\infty = 0.55$ ,  $Re = 5.65 \times 10^6$ ,  $\mu = 0.45$  and  $k = 0.3668$ ).

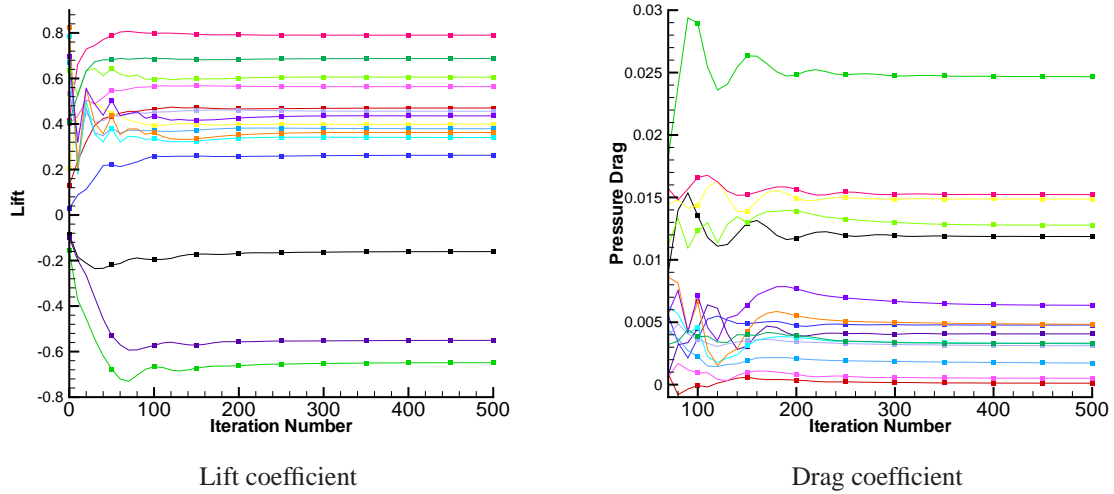


Figure 6: Convergence of the lift and drag coefficients for the 7-mode harmonic balance viscous dMdt case ( $M_\infty = 0.55$ ,  $Re = 5.65 \times 10^6$ ,  $\mu = 0.45$  and  $k = 0.3668$ ).

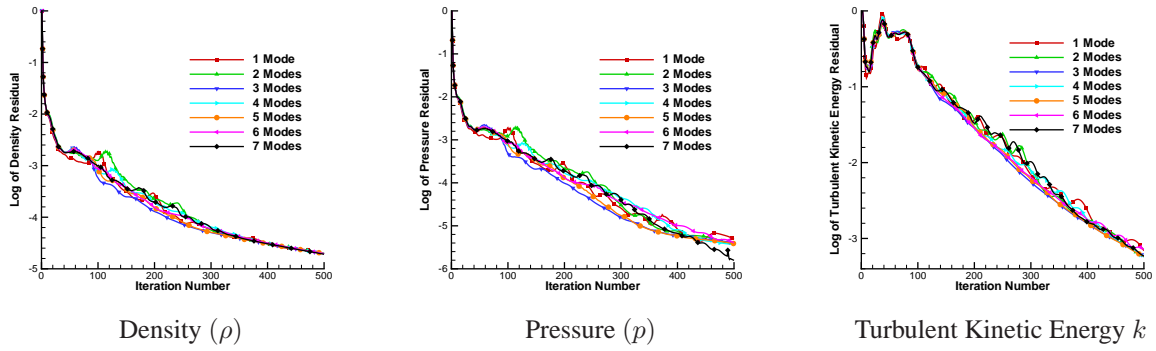


Figure 7: Convergence history of the Harmonic Balance method for the viscous dMdt case ( $M_\infty = 0.55$ ,  $Re = 5.65 \times 10^6$ ,  $\mu = 0.45$  and  $k = 0.3668$ ).

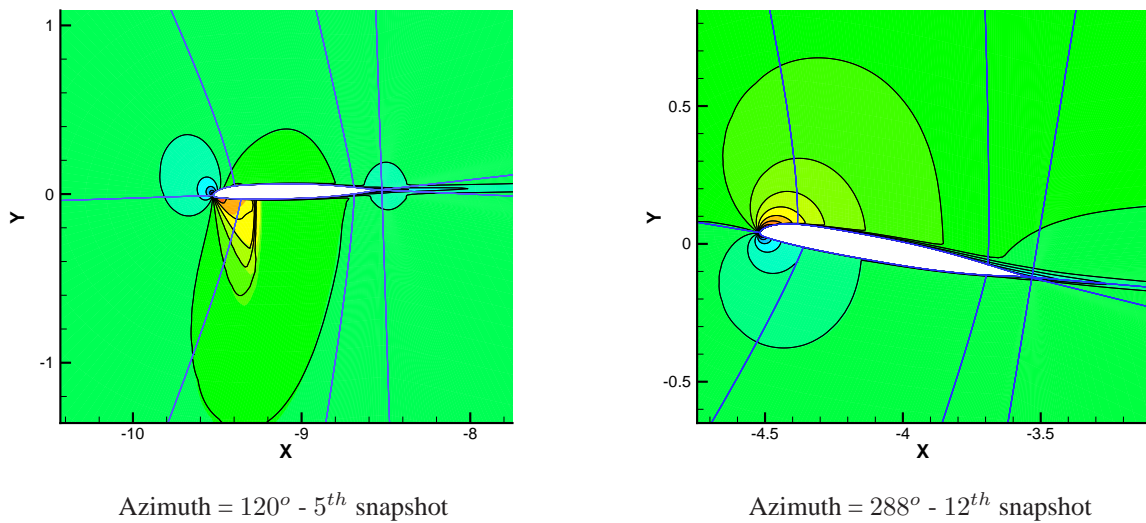
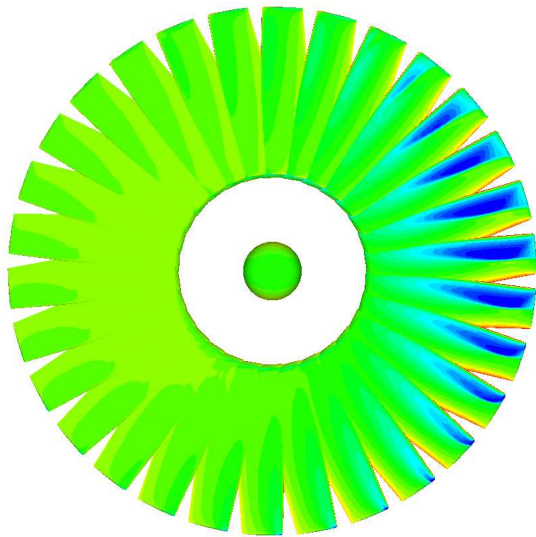
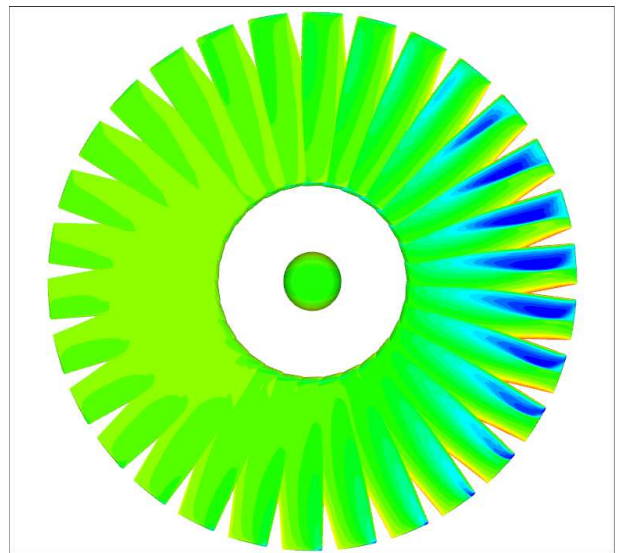


Figure 8: Comparison of the time marching solution Mach number (shaded contours) - and a 7 mode harmonic balance solution (black contours) for the viscous dMdt case ( $M_\infty = 0.55$ ,  $Re = 5.65 \times 10^6$ ,  $\mu = 0.45$  and  $k = 0.3668$ ).



Non linear inviscid time marching



7 Mode inviscid harmonic balance

Figure 9: Comparison of the surface pressure on the blades for the ONERA non-lifting rotor.

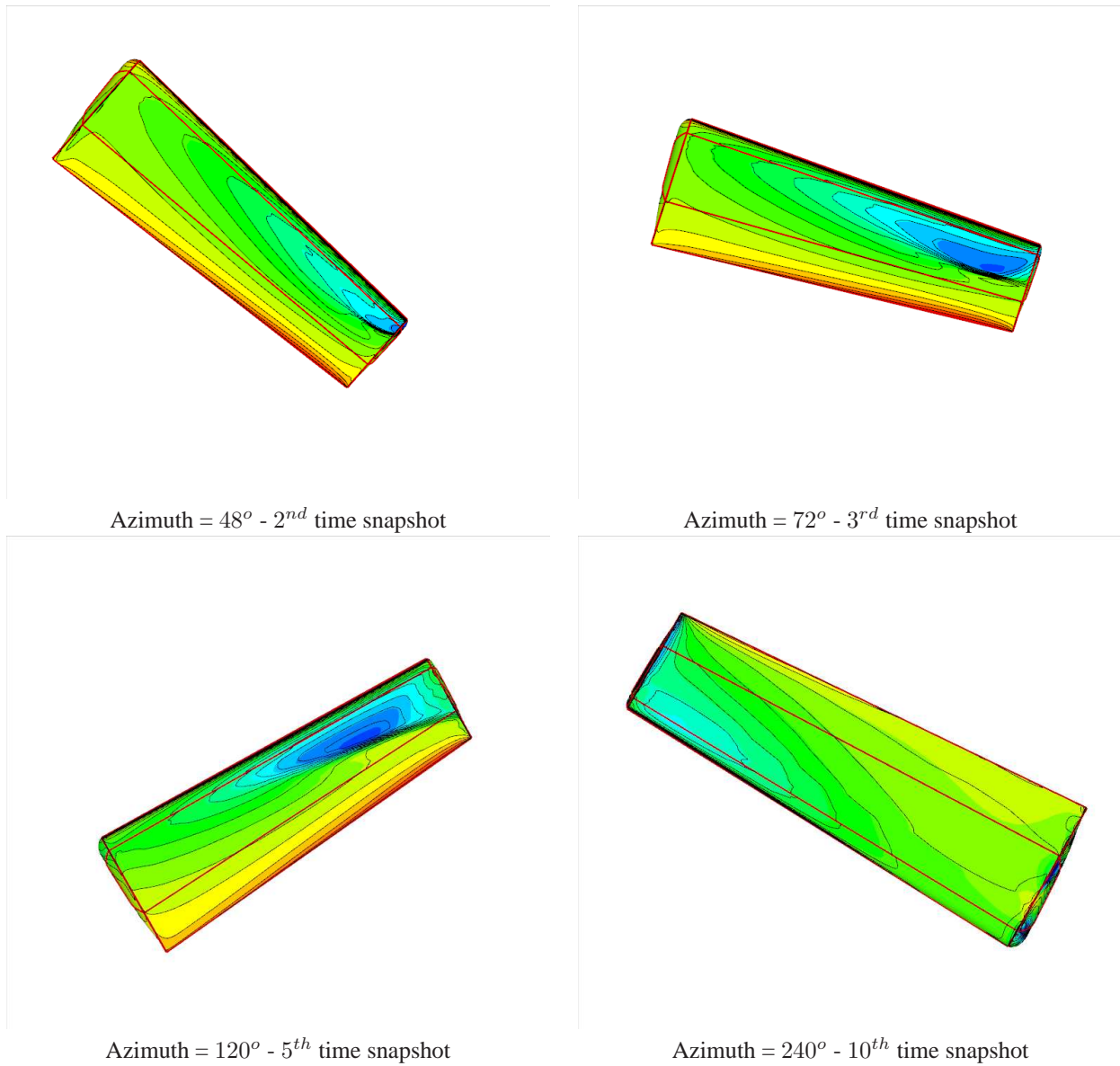


Figure 10: Comparison of the non linear pressure ( in colour) and a 7-mode harmonic balance pressure (black lines) for the flow field in the ONERA non-lifting rotor test case.

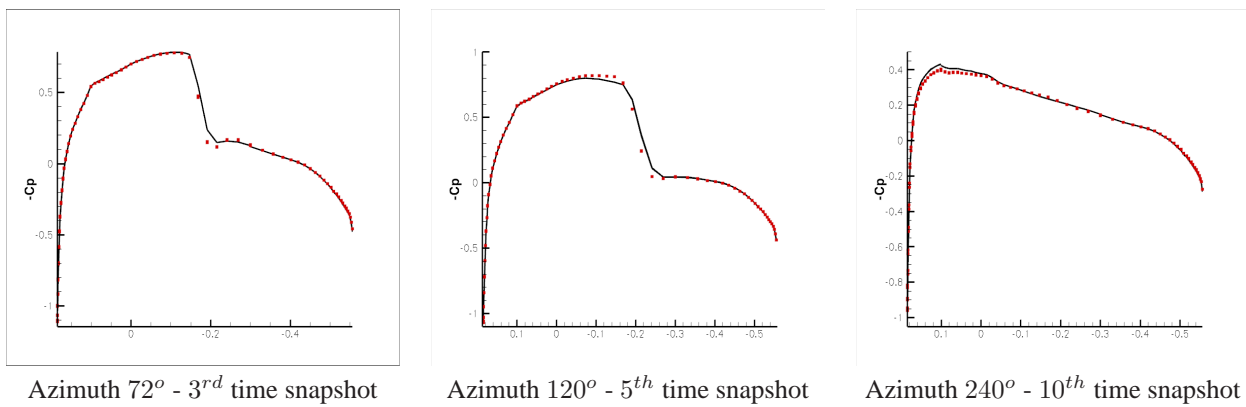


Figure 11: Comparison of the non linear Cp (black lines) and a 7-mode harmonic balance Cp (red squares) for the ONERA non lifting test case.



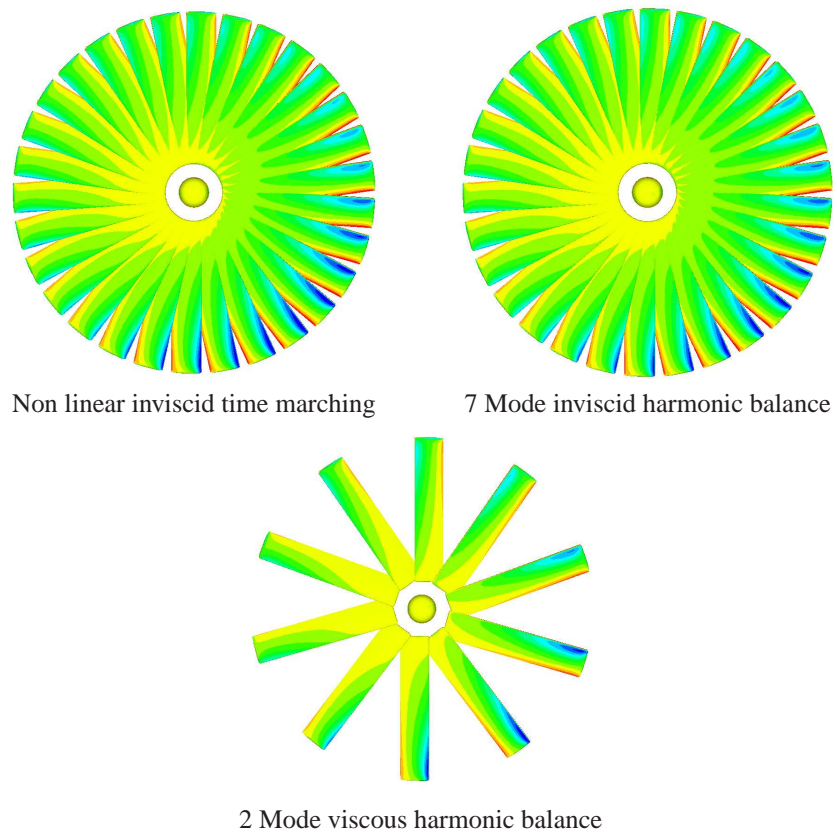


Figure 12: Comparison of the Surface pressure on the blades for the lifting rotor.

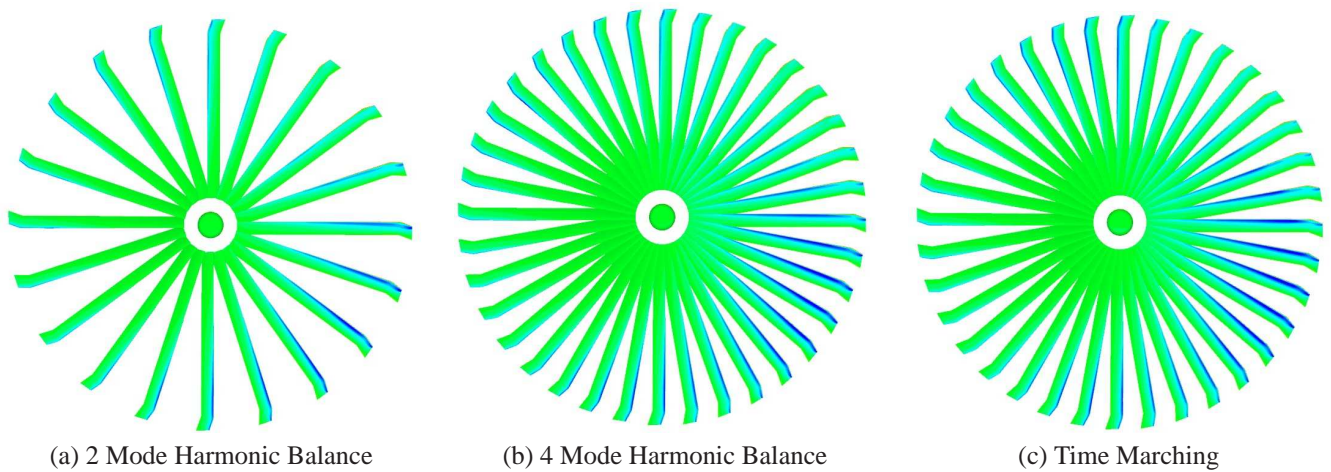


Figure 13: Harmonic balance and time marching results for the UH60 rotor in forward flight.

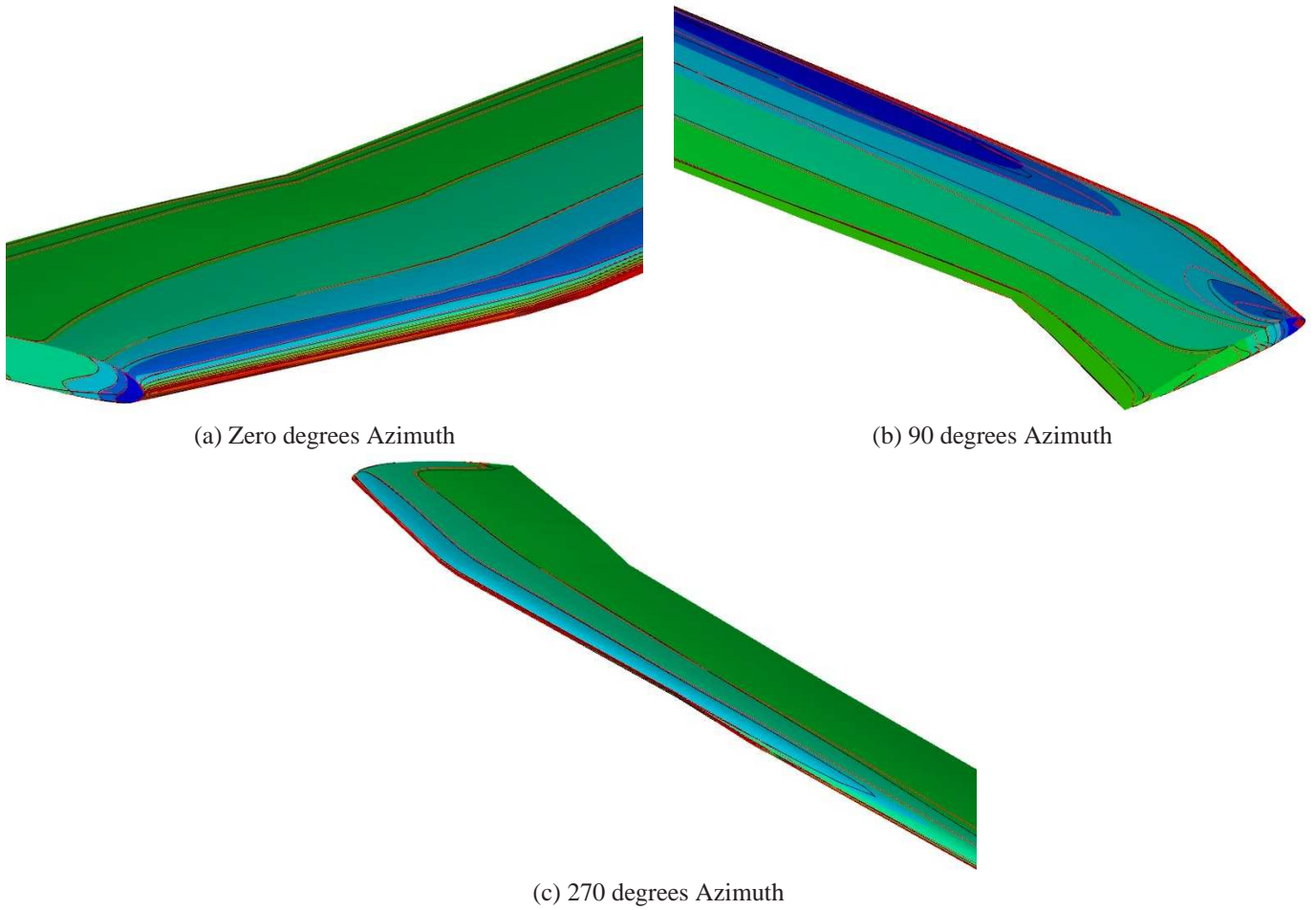
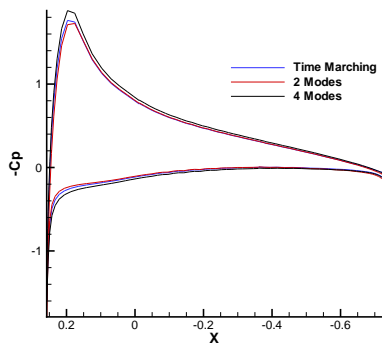
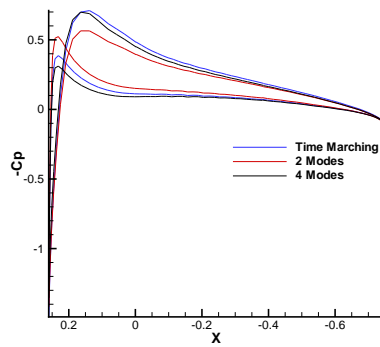


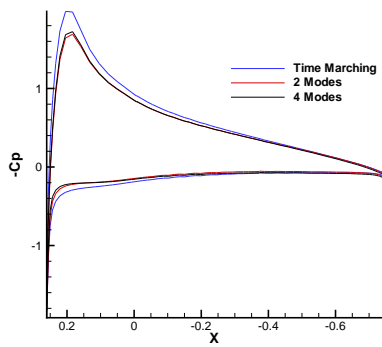
Figure 14: Harmonic balance and time marching results for the UH60 rotor in forward flight. The colour contours are the pressure from the time marching simulation, the red lines correspond to the 2-Mode solution, and the black lines to the 4-Mode solution.



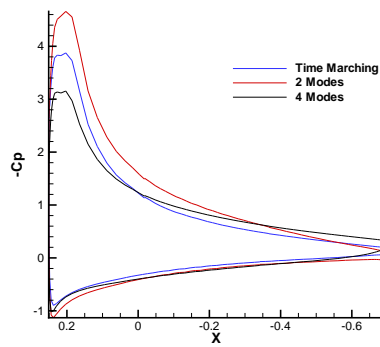
(a) Zero degrees Azimuth



(b) 90 degrees Azimuth

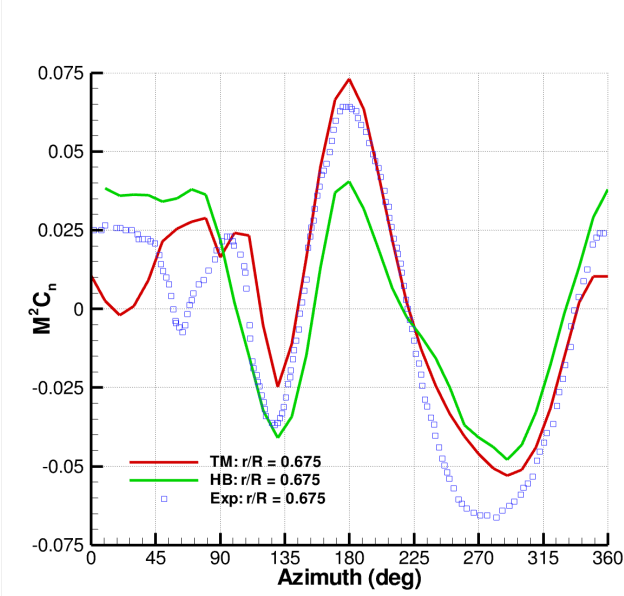


(c) 180 degrees Azimuth

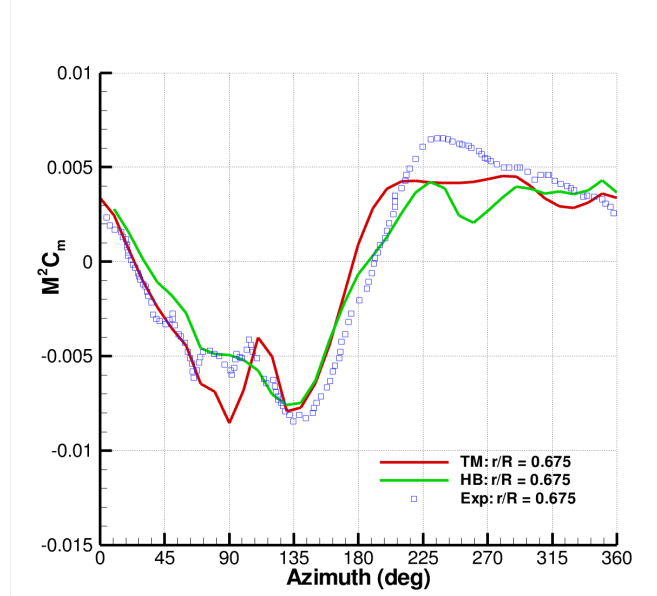


(d) 270 degrees Azimuth

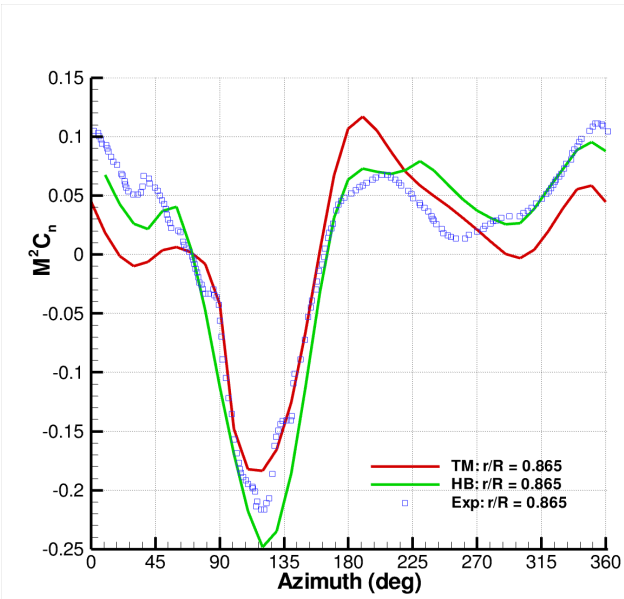
Figure 15: Harmonic balance and time marching results for the UH60 rotor in forward flight. The comparisons of the surface  $C_p$  are shown for the  $67.5\%R$  station.



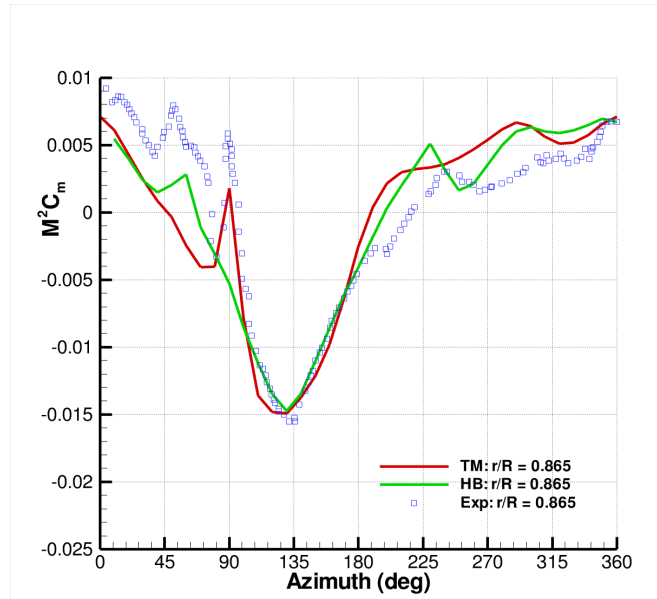
(a)  $M^2 C_n$   $r/R = 0.675$



(c)  $M^2 C_m$   $r/R = 0.675$



(a)  $M^2 C_n$   $r/R = 0.865$



(c)  $M^2 C_m$   $r/R = 0.865$

Figure 16: Comparison of the Mach squared scaled loads between the experimental data, the CFD Timing marching solution and the 4 mode Harmonic balance solution for the UH60 rotor in forward flight at two different span-wise stations.